Zn-Cu Alloy Nanofoams as Efficient Catalysts for the Reduction of CO 2 to Syngas Mixtures with a Potential-Independent H 2 /CO Ratio

Sarah Lamaison, David Wakerley, David Montero, Gwenaëlle Rousse, Dario Taverna, Domitille Giaume, Dimitri Mercier, Juliette Blanchard, Huan Ngoc Tran, Marc Fontecave, et al.

Zn-Cu alloy nanofoams as efficient catalysts for CO_2 reduction to syngas mixtures with potential-independent H_2:CO ratio

Sarah Lamaison[a], David Wakerley[a], David Montero[b], Gwenaëlle Rousse[c], Dario Taverna[d], Domitille Giaume[e], Dimitri Mercier[e], Juliette Blanchard[f], Huan Ngoc Tran[a], Marc Fontecave*[a] and Victor Mougel*[a]

Abstract: Alloying strategies are commonly used to design electrocatalysts that take on properties of their constituent elements. Herein, we explore the use of such a strategy to develop Zn-Cu alloyed electrodes with unique hierarchical porosity and tunable selectivity for CO_2 *vs.* H^+ reduction. By varying the Zn:Cu ratio, tailored syngas mixtures were attained with no other gaseous products, which we assign to preferential CO and H_2 forming pathways on the alloys. The syngas ratios were also significantly less sensitive to the applied potential in the alloys relative to pure metal equivalents; an essential quality when coupling electrocatalysis to renewable power sources of fluctuating intensity. As such, industrially-relevant syngas ratios were achieved at large currents (–60 mA) for extensive operating times (> 9 h), demonstrating the potential of this strategy for fossil-free fuel production.

Introduction

Electroreduction of CO_2 into energy-dense compounds such as carbon monoxide, formic acid, hydrocarbons and alcohols offers a promising route to store intermittent renewable energies. Multi-carbon products (ethanol, ethylene, propanol *etc.*) are the most valued outcome of such a process, representing a denser store of chemical energy. However, the multi-electronic and multi-protonic nature of the reactions at work commonly results in very high overpotential, low faradaic efficiency and complex product mixtures. This process is commonly carried out in aqueous media, with the anodic oxidation of water providing the source of protons and electrons. Yet, the use of aqueous electrolyte is highly challenging considering the kinetically and thermodynamically facile alternative reduction of H^+ to H_2. While significant efforts are currently being made to develop electrocatalysts promoting the direct CO_2 reduction to hydrocarbons or alcohols with limited activity for H^+ reduction, an equally attractive strategy is to take advantage of the produced H_2 to generate valuable gas mixtures, such as syngas, a combination of CO and H_2. Syngas can be used to produce hydrocarbons and alcohols through well-established industrial technologies. A two-step process that couples CO_2 electroreduction to syngas with its subsequent transformation to high added-value products has been proposed to be more favorable from an economic perspective since i) CO_2 reduction to CO occurs at moderate overpotentials and ii) a highly energy-demanding product separation step is not required.[1] However, one of the main prerequisites for the syngas generated is control over the H_2:CO ratio, that must meet different values depending on the reaction targeted: optimal H_2:CO ratios of 1.5-2.2 are typically required for methanol synthesis and the Fischer-Tropsch reaction; 3 for the methanation reaction; and 1 is typically required for hydroformylation and fine chemical synthesis.[1]

Fossil-fuel reforming reactions are currently the largest source of syngas; however these processes generate specific H_2:CO ratios (Figure 1) and are based on non-renewable feedstocks. Adjusting these ratios requires an additional energy-demanding water-gas-shift reaction.[1] In this context, electrochemical syngas generation is a more versatile and sustainable alternative, allowing a broad range of H_2:CO ratios to be produced from renewable precursors (H_2O and CO_2).[2, 3] The electrochemical conversion of CO_2 to syngas is particularly relevant in the context of renewable electricity conversion, which requires the design of electrolytic devices tolerant to the significant variations of power provided by intermittent energy sources, such as photovoltaic panels. Nevertheless, to the best of our knowledge all the electrocatalytic systems for syngas generation present a significant variation of the H_2:CO ratio with applied potential, preventing an efficient coupling with such sources of electricity.

[a] Sarah Lamaison, Dr. David Wakerley, Dr. Huan Ngoc Tran, Prof. Marc Fontecave, Dr. Victor Mougel
Laboratoire de Chimie des Processus Biologiques, CNRS UMR 8229, Collège de France, Sorbonne Université 11 Place Marcelin Berthelot, 75231 Paris Cedex 05, France
E-mail: marc.fontecave@college-de-france.fr ; victor.mougel@college-de-france.fr
[b] David Montero
Institut des Matériaux de Paris Centre, FR 2482, Sorbonne Université, 4 place Jussieu, 75005 Paris, France
[c] Dr. Gwenaëlle Rousse
Laboratoire de Chimie du Solide et Energie, UMR 8260, Collège de France, Sorbonne Université, 11 Place Marcelin Berthelot, 75231 Paris Cedex 05, France.
[d] Dr. Dario Taverna
Institut de Minéralogie, de Physique des Matériaux et de Cosmochimie, CNRS UMR 7590, MNHN, IRD, Sorbonne Université, 4 place Jussieu, 75005 Paris, France.
[e] Dr. Domitille Giaume, Dr. Dimitri Mercier
Chimie ParisTech, PSL Research University, CNRS, Institut de Recherche de Chimie de Paris, 11 rue Pierre et Marie Curie, 75005 Paris, France
[f] Dr. Juliette Blanchard
Sorbonne Université, CNRS, Laboratoire de Réactivité de Surface, LRS UMR 7197, F-75005, Paris, France

Supporting information for this article is given via a link at the end of the document.

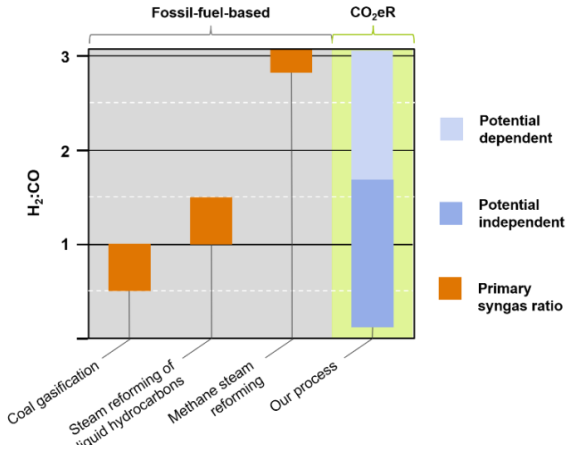

Figure 1. H_2:CO ratios reachable using fossil-fuel-based techniques *versus* the CO_2 electroreduction (CO_2eR) process presented in this work. Data for fossil-fuel-based processes are taken from ref [1]. Primary syngas ratio refers to the obtained products without additional gas-shift reactions to readjust the ratio.

An effective syngas generating system must therefore meet several key parameters:

1. The modulation of the H_2:CO ratio must not depend on the potential applied; materials that can independently fine-tune the transfer coefficients for the formation of H_2 and CO must be chosen.
2. The system must operate in a regime where the current is not limited by the diffusion of reactants; CO_2 is present in a very low concentration in aqueous solutions and therefore a system maximizing reactant mass transfer is mandatory.
3. The chosen system must be selective for syngas production only, *i.e.* the typical concomitant formation of formic acid must be minimized.

Previous reports have focused on monometallic molecular[4-6] and heterogeneous catalytic systems,[7-15] showing simultaneous CO and H_2 production, but single catalytic sites offer limited possibilities to tune catalyst selectivity. Introducing a second metal site offers an extra degree of freedom in catalyst design and thereby offers the best route to address the above criteria.[12, 16, 17] By combining two metals, one with a high propensity for CO_2 reduction and another for proton reduction, ratios of syngas can easily be attained by altering the ratio of the constituent metals.[12]

Herein, we present a series of high-surface area dendritic foams comprised of Zn alloyed with varied amounts of Cu. The foams are generated through a facile co-electrodeposition of Zn with sub-stoichiometric amounts of Cu. The Cu-doping first plays a major role in the growth of the catalysts; Cu salts in the deposition precursor solution triggers the growth of high surface area three-dimensional porous dendritic materials via a hydrogen-evolution-assisted electrodeposition approach,[18, 19] not possible with Zn alone. The incorporated Cu then presents sites for hydrogen evolution in the material such that H_2:CO ratios are found to correlate directly to the Cu:Zn ratio in the catalyst. The resultant porous structures also allow fast diffusion of species to the micropores, keeping the H_2:CO ratio constant in a wide potential range by preventing mass transfer limitations. Syngas production could thus be achieved at currents up to – 45 mA at – 1.2 V *vs.* RHE using 1 cm^2 flat-Zn supported catalysts. This strategy could be extended to a 1 cm^3 Zn-foam-supported catalyst, which exhibited syngas production over multiple hours, reaching up to –60 mA at –1.1 V *vs.* RHE.

Results and discussion

Zn:Cu Alloy Growth and Characterization

Dendritic Zn:Cu foam electrodes were generated by applying high current density (0.5 $A.cm^{-2}$) to 1 cm^2 Zn plates immersed in a 0.5 M H_2SO_4 aqueous solution of metal precursors. The total metal salt concentration was kept constant and equal to 0.1 M but distributed between X% of 'doping' $CuSO_4$ and (100–X)% $ZnSO_4$ with X varying between 0% and 35%. These electrodes are labelled $Zn|ZnSO_4^{(100-X)\%}CuSO_4^{X\%}$ in the following sections. Scanning electron microscopy (SEM) reveals that the presence of $CuSO_4$ in the precursor mixture, even below 5%, promotes high nano- and meso-porosity within the Zn-based 'fern-like' structures, which otherwise grow in a low-surface-area stacked configuration (Figure 2 and Figure S1).

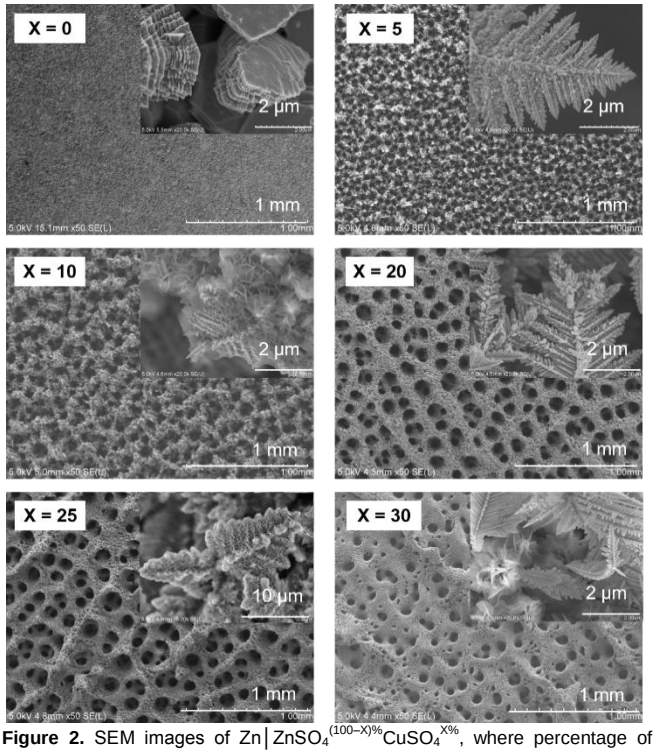

Figure 2. SEM images of $Zn|ZnSO_4^{(100-X)\%}CuSO_4^{X\%}$, where percentage of $CuSO_4$ (X) is 0, 5, 10, 20, 25 and 30, as indicated in the top-left corner of corresponding images.

Angled SEM images of the electrode cross-sections reveal that deposit thickness increases by about an order of magnitude between 1% $CuSO_4$ and 10% $CuSO_4$ doping (Figure S2), reaching values of ~150 µm in the latter case, but only

marginally increases at higher doping levels. All alloys showed enhanced porosity, confirmed through BET measurements (Table 1); the electrodes prepared with the highest Cu doping display the highest surface area. Areas as high as 27.4 m^2 g^{-1} were reached, corresponding to a roughness factor (RF) of *ca.* 25 once normalized by the mass of electrodeposited material. This marks a substantial improvement over the RF = 1.12 of bulk Zn foil previously recorded using atomic force microscopy.[20]

Elemental composition of the electrodeposited alloys was probed by energy-dispersive X-ray spectroscopy (EDS) and inductively coupled plasma - atomic emission spectroscopy (ICP-AES) measurements (Table 1 and Figure S3-S9). The incorporation of Cu in the materials was confirmed at each loading investigated, and ICP-AES measurements revealed that the Cu:Zn ratio in the material is typically 1.5 times higher than the Cu:Zn ratio present in the metal sulfate precursor solution (Table 1), in agreement with the thermodynamically preferential reduction of Cu^{2+} *vs.* Zn^{2+}. The bulk Cu content determined for each electrode hence differs from the Cu content 'X' used for the naming $Zn|ZnSO_4^{(100-X)\%}CuSO_4^{X\%}$ of the electrodes which refers to the content in $CuSO_4$ salt initially introduced in the precursor solution.

Table 1. Relationship between the $CuSO_4$ percentage in the precursor solution, the subsequent percentage of Cu incorporated in the electrode (bulk, determined by ICP-AES), at its surface (determined by XPS) and associated BET surface area and roughness factor (RF).

Electrode	%$CuSO_4$	% Cu (bulk)	% Cu (surface)	BET [$m^2.g^{-1}$]	RF
$Zn\|ZnSO_4^{95\%}CuSO_4^{5\%}$	5	6.5±0.5	1	1.3	1.3
$Zn\|ZnSO_4^{90\%}CuSO_4^{10\%}$	10	13±1	2	3.8	3.5
$Zn\|ZnSO_4^{80\%}CuSO_4^{20\%}$	20	32±3	n/d	16.9	15
$Zn\|ZnSO_4^{75\%}CuSO_4^{25\%}$	25	39.5±4	n/d	14.6	13
$Zn\|ZnSO_4^{70\%}CuSO_4^{30\%}$	30	59.3±6	12	27.4	25

To gain deeper insight into the bulk and surface composition and mixing pattern of the deposits, known to have a significant influence on the catalyst selectivity[16], the electrode materials were analyzed using X-ray diffraction spectroscopy (XRD), X-ray Photoelectron Spectroscopy (XPS) and high-resolution transmission electron microscopy (HR-TEM). Diffractograms for $Zn|ZnSO_4^{(100-X)\%}CuSO_4^{X\%}$ electrodes confirm the strong correlation of alloy content and the relative metal stoichiometry of the soluble precursors (Figure 3). At low loading ($X \leq 10$), the XRD patterns of the corresponding $Zn|ZnSO_4^{(100-X)\%}CuSO_4^{X\%}$ structures show hexagonal-Zn phases with slight variations of lattice parameters, suggesting a solid solution of Cu in these materials, as well as additional hexagonal phases attributed to a $Cu_{0.2}Zn_{0.8}$ alloy. With increasing Cu content ($10 < X \leq 30$), diffraction patterns attributed to cubic Cu_5Zn_8 and Cu_3Zn are observed. In some samples, further analysis at low diffraction angles revealed the presence of a low amount of namuwite ($Zn_{3.2}Cu_{0.8}SO_4(OH)_6(H_2O)_4$) at the surface of the electrodes (Figure S10). This insoluble sulfate probably stays at the surface of the electrode after synthesis. It however disappears during electrolysis, as exemplified by the comparison of $Zn|ZnSO_4^{70\%}CuSO_4^{30\%}$ XRD patterns before and after 3 hours of electrolysis (Figure S10), without affecting the morphology of the electrode, as corroborated by a drop in S content measured in SEM-EDX (Figure S3-S9).

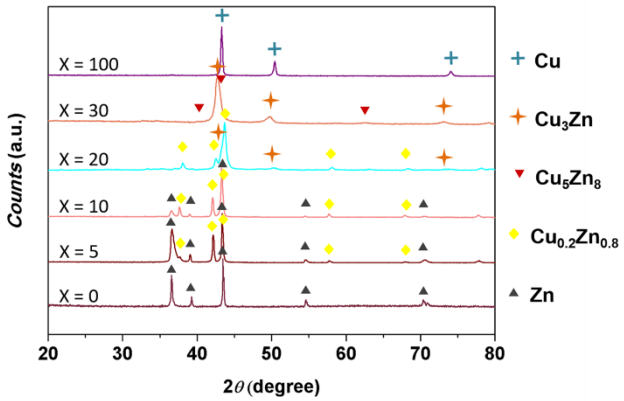

Figure 3. Powder X-ray diffraction patterns of $Zn|ZnSO_4^{(100-X)\%}CuSO_4^{X\%}$ where percentage of $CuSO_4$ (X) is varied between 0 and 100.

X-ray Photoelectron Spectroscopy (XPS) of $Zn|ZnSO_4^{(100-X)\%}CuSO_4^{X\%}$ electrodes confirms that both Cu and Zn are present at the surface of the electrode at low and high Cu loading (Table 1). The quantification of the relative Cu:Zn surface ratio indicates that the surface Cu content is around 6 times lower than the bulk Cu content determined by ICP-AES. This Cu:Zn surface ratio is unchanged before and after electrolysis (Figure S11).

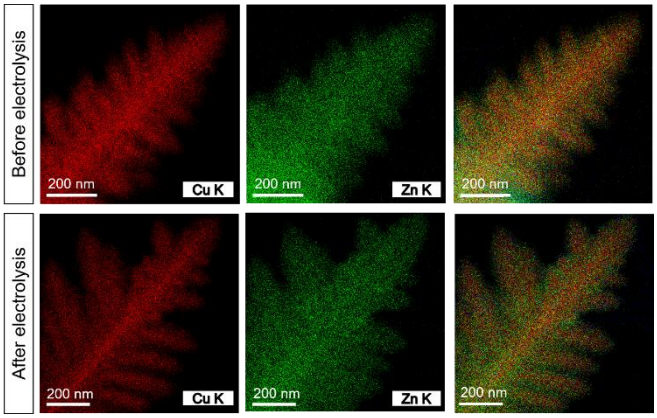

Figure 4. STEM-EDXS analysis of a $Zn|ZnSO_4^{90\%}CuSO_4^{10\%}$ fern-shaped structure before and after 3 h of electrolysis at –1.0 V *vs.* RHE in CO_2-saturated 0.1 M $CsHCO_3$. The overlay (far right) shows Cu in red, Zn in green and O in blue.

High Resolution TEM (HRTEM) combined with elemental mapping with Scanning Transmission Electron Microscopy-Energy-Dispersive X-ray Spectroscopy (STEM-EDXS) confirmed that homogeneous distribution of Cu and Zn was present even at the nanoscale features of the dendrite as illustrated in the typical 'fern-shaped' structure in Figures 4 and S12. Comparison of the microstructures before and after use in electrocatalytic

conditions (Figure 4, S3-S12), shows no change in the atomic distribution of the metal sites, demonstrating high structural stability of this surface. A sporadic distribution of O is seen by STEM-EDXS on the surface of the structure (more visible at lower magnification, Figure S12), which is not present after electrolysis, and is thus assigned to the aforementioned namuwite phase.

The considerable influence of even small quantities of Cu on the overall porosity, surface morphology, as well as its facile intercalation within the Zn structure, suggests that Cu is not only a doping agent, but also has a strong structural role. We assign this to the 1.1 V more positive reduction potential of Cu^{2+} with respect to that of Zn^{2+},[21] promoting more rapid growth by providing seeding sites for Zn deposition, as confirmed by the higher Cu content in the bulk of the dendrites than at their surface. Proton reduction to H_2 is also exacerbated by the Cu surface sites, ensuring constant H_2 evolution during deposition, which promotes growth of macroporous structures. We explored this preparation protocol from an industrial application perspective, which proved scalable and versatile: deposition could be applied equally well to Zn and Cu plates, as well as Zn foam. Also, homogeneous electrodes as large as 8 cm^2 could be obtained with no decrease in homogeneity or change in morphology (Figure S13-S14).

Electrochemical syngas generation

Electrocatalytic activity for syngas production of the $Zn|ZnSO_4^{(100-X)\%}CuSO_4^{X\%}$ electrodes was investigated in a two-compartment H-type electrolyzer equipped with anion exchange membrane under constant CO_2 flow (20 mL min^{-1}). In order to limit the competitive H_2 production and explore a broader range of H_2:CO ratios, electrolyses were carried out in 0.1 M $CsHCO_3$ electrolyte (pH=6.8), as previous reports demonstrated that large cations in the electrolyte favor CO_2 *vs.* proton reduction.[22, 23] 1 cm^2 working electrodes were used here as we found that the properties measured on very small electrodes (< 0.5 cm^2) do not appear to scale up correctly when increasing the geometric surface area of the electrode, likely as a consequence of the significant thickness of the deposit (≥ 100 µm for X≥ 5). Similarly, we did not apply iR-drop correction, as *operando* changes in interface resistivity of the electrode, especially those with large surface areas, led to inaccurate corrections to the applied potential, particularly considering that first-row transition metal surfaces have a tendency to exist as resistive oxides before application of negative potentials. These corrections also ignore resistances that would be intrinsic to the electrode when used in a full electrolyzer cell, and which must be accounted for as industrial application is considered.

Figure 5a presents the H_2:CO ratios with respect to Zn:Cu proportions in the precursor mixture and the applied potential. The corresponding partial current densities for total syngas production are shown in Figure 5b. At each potential and with each Zn-Cu material investigated, CO and H_2 were the sole products in the gas phase and accounted for ~80% of the total products formed in all cases (Figure S15). Formic acid was also formed, with FE at around 20% at low Cu loadings and below 2 % at high loading (Figure S16). Significantly, for all $Zn|ZnSO_4^{(100-X)\%}CuSO_4^{X\%}$ electrodes (with X chosen between 5 and 30), the syngas composition is a characteristic of the electrode composition, and is rather independent of the applied potential. The opposite is observed for monometallic Zn electrodes, as is shown by the large variations of H_2:CO ratio as a function of applied potential, even when the electrode is nanostructured (Figure 5a).

The selectivity of the alloys differs from both Cu-based catalysts (typically producing multi-carbon products) and Zn-based catalysts (typically producing CO and formic acid).[24] This disparity can be rationalized according to the analysis of Rossmeisl *et al.*[25] In the latter, the calculated binding energies of H* and COOH* (selected as relevant intermediates in the production of H_2, CO and HCOOH) were demonstrated as good descriptors for the selectivity of metallic electrodes during CO_2 reduction. Reasoning here on the individual metals, we notice that the introduction of Cu to Zn would aid H_2 evolution, as Cu possesses a lower hydrogen binding energy than Zn ($\Delta E_{Cu\text{-}H^*}$ = 0.0 eV *vs.* $\Delta E_{Zn\text{-}H^*}$ = +0.5 eV). On the other hand CO evolution should not be strongly impacted by the alloying strategy, as the adsorption energy of COOH* on Zn and Cu are comparable ($\Delta E_{Cu\text{-}COOH^*}$ = +0.5 eV compared to $\Delta E_{Zn\text{-}COOH^*}$ = +0.7 eV). This also explains the decrease in formic acid production with increased Cu incorporation (Figure S16), as this reaction occurs on metal sites with COOH* binding energy lower than/ similar to H* (*i.e.* a positive/near zero $\Delta E_{H^*} - \Delta E_{COOH^*}$), which is not the case on Cu ($\Delta E_{Cu\text{-}H^*} - \Delta E_{Cu\text{-}COOH^*}$ = –0.5 eV *vs.* $\Delta E_{Zn\text{-}H^*} - \Delta E_{Zn\text{-}COOH^*}$ = –0.2 eV).[25] Multi-carbon products are similarly not seen as their formation requires stabilized bound CO* intermediates, which are disfavored by the weaker CO* binding energy of Zn in the alloy ($\Delta E_{Zn\text{-}CO^*}$ = –0.15 eV compared to $\Delta E_{Cu\text{-}CO^*}$ = –0.5 eV), offering a pathway for CO release.[25] Zn and Cu would therefore synergistically increase the other metal's selectivity, by essentially 'turning off' their secondary reactions. Control over product selectivity is thus afforded through facile variation of the Zn:Cu content of the alloy (Figure 5a).

These findings do not corroborate with previous studies of Cu-Zn alloys that propose the use of a Zn co-catalyst as an *in situ* source of CO to enhance further ethanol production on Cu sites.[26] This discrepancy may be explained by the difference in the deposition regimes used; in the latter case, Cu content is substantially higher and as such contains extended phases of multiple Cu sites that likely behave similarly to bulk copper.[27]

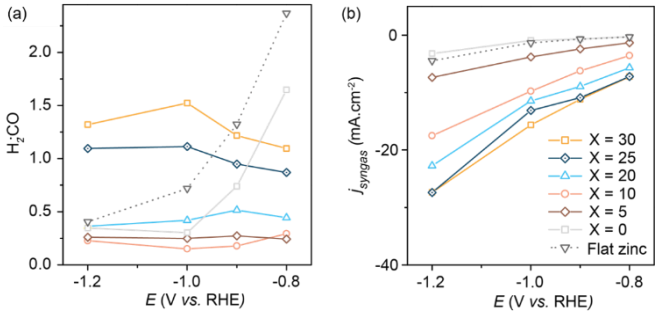

Figure 5. (a) Molar H_2:CO ratios and (b) corresponding total partial current densities for syngas production obtained at various potentials using $Zn|ZnSO_4^{(100-X)\%}CuSO_4^{X\%}$, where percentage of $CuSO_4$ (X) is 0, 5, 10, 20, 25 and 30.

The Zn-Cu alloy composition thus provides a way to obtain syngas with a broad range of H_2:CO ratios from 0.2 to 1.6. These ratios encompass typical values obtained using fossil-fuel-derived syngas (petrol and coal steam reforming or gasification), and can be directly used for hydroformylation, the Fischer-Tropsch reaction or methanol synthesis. Higher H_2:CO ratios (up to 3.65), in the range of those required for the methanation reaction could also be obtained when using electrodes with higher Cu loading (X> 30), yet losing the invariance of the ratio with applied potential observed at lower loadings (Figure S17).

Furthermore, the electrodes showed remarkable stability over time. Stable currents and selectivity were observed over >3 h constant potential electrolysis on Zn | $ZnSO_4^{90\%}CuSO_4^{10\%}$ (Figure S18). Moreover, powder XRD patterns, XPS, SEM, STEM-XEDS and HR-TEM images after operation demonstrate that the composition and nanoscale morphology are preserved during electrolysis (Figure S3-S12).

The stability and scalability of the electrode were finally investigated on a higher surface area support to target industrially relevant currents. Depositing $ZnSO_4^{90\%}CuSO_4^{10\%}$ onto commercially-available Zn foam (Mesh 4, 1 cm^3) generated a highly-structured surface referred to as Zn foam | $ZnSO_4^{90\%}CuSO_4^{10\%}$, similar to those deposited on flat Zn (Figure S19), and afforded stable currents in the range of –50 to –60 mA.

As proof of the electrode's amenability to versatile syngas production in real-world conditions, we tested its response to the potential variations commonly observed while coupling the electrolyzer to an intermittent source of energy, such as solar panels. The applied potential was varied during electrolysis with the aforementioned foam over a 300 mV range, over which time the electrode maintained a stable H_2:CO ratio (Figure 6). In total, the system was operated for more than 9 h without any decline in activity or selectivity, nor evidence of structural degradation (Figure S19). It should be noted that, while independent with respect to the applied potential in both cases, the H_2:CO ratio observed using the Zn foam differs from that obtained using flat Zn as a support. This likely is a consequence of the very different diffusion and convection regime between these two supports, affecting the local concentration of the reactants at the electrode and the final H_2:CO ratio.

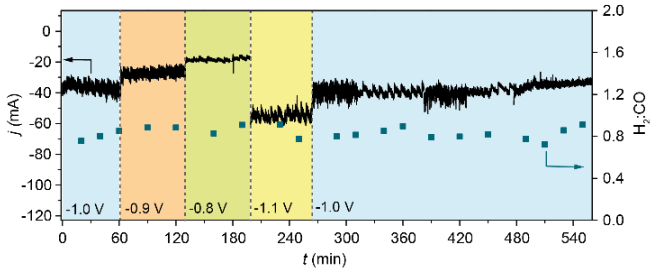

Figure 6. Long-term electrolysis of a high surface area Zn foam | $ZnSO_4^{90\%}CuSO_4^{10\%}$ in CO_2-saturated 0.1 M $CsHCO_3$. Varying the applied potential to mimic the foreseeable voltage fluctuations delivered by an intermittent renewable power source. Catalytic current is reported on the left axis (black) and corresponding H_2:CO ratio on the right axis (bulk symbols). Electrolyte was changed between each potential and roughly every hour beyond 260 minutes, causing slight signal variations.

Conclusions

In this work, we have illustrated the use of a mixed-phased Zn-Cu alloying strategy for the one-step fabrication of a standalone material with tunable selectivity for the H^+ reduction and CO_2 reduction reactions. The doping strategy not only provided fine control over catalytic selectivity, but the presence of easily-reduced Cu aided the growth of highly porous Zn-Cu alloys through seeding and hydrogen-evolution-assisted electrodeposition. H_2:CO ratios could be tuned from 0.2 to 3.65 and hence adjusted to desired ranges for syngas usage with industrially relevant currents. The catalyst activity could be related directly to the binding strength of the Cu and Zn atoms to key catalytic intermediates; a strategy that is applicable to future development of mixed-metal electrodes.

Finally, the unique ability of these materials to maintain a constant H_2:CO ratio over a broad range of applied potentials provides a new practical system to convert CO_2 to industrially relevant products using intermittent, renewable energy sources.

Experimental Section

Electrode preparation

Unless stated otherwise, electrodes were prepared on 1 cm^2 Zn foil (GoodFellow, 99,99+%, 1 mm) successively polished by P1200, P2400 emery paper and Al-powder followed by sonication in water before deposition. When the support employed was Cu, the same mechanical polishing procedure was applied on a 1 cm^2 Cu foil (GoodFellow, 99,999%, 1 mm). Each electrode was then immersed in a 0.5 M H_2SO_4 aqueous solution of 0.1 M metal salt apportioned between X% $CuSO_4$ and (100–X)% $ZnSO_4$ depending on the targeted Cu content and exposed to – 0.5 $A.cm^{-2}$ for 160 s using a three-electrode set-up with an Ag/AgCl (KCl sat.) reference and Pt counter. In the case of the foam, 1 A was applied for 160 s. In each case the electrode was immediately rinsed with milliQ water and air-dried after deposition.

$CuSO_4 \cdot 5H_2O$ (99.9%) and H_2SO_4 (99.8%), were purchased from Sigma-Aldrich and used without further purification. $ZnSO_4.7H_2O$ (99.5%) was purchased from Roth chemicals.

Structure characterization

Imaging and EDX (Energy dispersive X-Ray spectrometry) were performed on a SU-70 Hitachi FEGSEM fitted with an X-Max 50 mm^2 Oxford EDX spectrometer. The imaging setup was 5 kV in order to observe surface features. Setup for quantitative analysis and mapping was 15 kV. Standards used as a reference for this voltage were purchased at Geller microanalytical laboratory (Boston, MA). Volume analyzed at this voltage is approximatively a sphere with diameter of ~700 nm. This value was calculated with Single Scattering Monte Carlo Simulation. Transmission electron microscopy images and chemical maps were acquired with a Jeol 2100F microscope operated at 200 kV. Chemical maps were acquired in STEM mode with the same microscope, equipped with Jeol system for X-ray detection and cartography. The elemental compositions of metallic electrodes

were verified with ICP-AES in a ThermoFisher iCAP 6000 device after dissolution of the metallic structures in 20% HNO_3 (Sigma-Aldrich, 65%).

Surface areas were obtained from the analysis of Kr sorption isotherms measured on a BelSorp Max set-up at 77 K. Prior to the measurement, samples were treated under vacuum at 130°C during at least 7 h. Surface areas were estimated using the BET model (Kr cross-sectional area 0.210 nm^2). The value derived from BET measurement, reported in $m^2.g^{-1}$, was converted to $cm^2.cm^{-2}_{geometric}$ by multiplying it by the mass of deposited electrode onto the 1 cm^2 flat Zn support. This provided a roughness factor (RF), as defined by the *IUPAC* GoldBook.[28]

Powder X-ray diffraction measurements were performed in Bragg-Brentano geometry using a BRUKER D8 Advance diffractometer with Cu Kα radiation ($\lambda K\alpha 1$=1.54056 Å, $\lambda K\alpha 2$=1.54439 Å) and a Lynxeye XE detector.

XPS characterization was performed using a Thermo ESCALAB 250 X-Ray photoelectron spectrometer with a monochromatic Al-Kα X-ray source ($h\nu$ = 1486.6 eV) operating at a pressure around 2×10^{-9} mbar. The analyzer pass energy was 50 eV for survey spectra and 20 eV for high-resolution spectra. The spectrometer was calibrated using Au 4f7/2 at 84.1 eV. Charging effects were not compensated during analysis. Spectra were recorded and analyzed using Thermo Avantage software version 5.966.

Electrochemical performance testing

Electrocatalytic measurements and constant potential electrolysis were carried out using a Bio-logic SP300 potentiostat. A H-type cell was used with the two compartments being separated by an anion exchange membrane (AMV Selemion^{TM}, ACG Engineering) with an inter-electrode distance of 6 cm between the working and Pt counter and an Ag/AgCl reference (saturated KCl) placed at 0.5 cm from the working. 0.1 M $CsHCO_3$ (Sigma-Aldrich, 99.9%) aqueous solution was used as both anolyte and catholyte, the latter being CO_2-saturated preceding the experiment (CO_2, Linde, HiQ 5.2) until the catholyte pH reached 6.8. During the electrolysis, CO_2 was constantly bubbled at 20 mL min^{-1} through a frit at the bottom of the cathodic chamber and generated gaseous products and excess CO_2 were flowed to the gaseous inlet of a gas chromatograph for online measurement.

Potentials are reported against the Reversible Hydrogen Electrode (RHE) according to the relationship *E vs. RHE = E vs.* Ag/AgCl + 0.197+0.059*pH.

Products characterization

H_2 and gaseous CO_2 reduction products were analyzed by a gas chromatography set-up (GC, Multi-Gas Analyzer #5 SRI Instruments) equipped with Haysep D and MoleSieve 5A columns, thermal conductivity detector (TCD) and flame ionization detector (FID) with methanizer using Argon as a carrier gas. GC was calibrated using a standard gas mixture containing 2500 ppm of H_2, CO, CH_4, C_2H_4, C_2H_6, C_3H_6, C_3H_8, C_4H_8 and C_4H_{10} in CO_2 (Messer). The liquid-phase products were quantified using ionic exchange chromatography (for oxalate – 883 Basic IC, Metrohm) and NMR spectroscopy (Bruker AVANCE III 300 spectrometer).

Faradaic efficiencies (*FE*) were calculated according to the following formula:

$$FE_{product} = \frac{n_e * n_{product} * F}{Q}$$

Where $n_{product}$ [mol] is the quantity of analyzed product, n_e [no unit] is the number of electrons involved in the formation of this product, F is the Faraday's constant equal to 96485 $C.mol^{-1}$ and Q is the corresponding passed charge. Partial current density for syngas production was calculated as follows:

$$j_{syngas} = (FE_{H2} + FE_{CO}) * j$$

where j refers to the total current density [$mA.cm^{-2}$].

Acknowledgements

S.L was supported by a doctoral fellowship from *Le Corps des Ponts, des Eaux et des Forêts.* V.M. acknowledges financial support from CNRS-Cellule Energie and Fondation of Collège de France for the acquisition of the GC equipment. D. W. was supported by an Idex PSL grant (ANR-10-IDEX-001-02 PSL★). We thank Dr. Andrei Nossov (LCMPC, UMR 7574, UPMC) for BET measurements and fruitful discussions. FEGSEM & EDX instrumentation was hosted at the Institut des Matériaux de Paris Centre (IMPC FR2482) and was funded by Sorbonne Université, CNRS and by the C'Nano projects of the Région Ile-de-France. We also thank Yves Dupraz (CIRB, UMR 7241, Collège de France) for assistance in electrode fabrication.

Keywords: CO_2 reduction • Syngas • Catalysis • Zn-Cu alloys • Electrolysis

[1] S. R. Foit, I. C. Vinke, L. G. J. de Haart, R.-A. Eichel, *Angew. Chem. Int. Ed.* **2017**, *56*, 5402-5411.

[2] R. Francke, B. Schille, M. Roemelt, *Chem. Rev.* **2018**, *118*, 4631-4701.

[3] T. Zheng, K. Jiang, H. Wang, *Adv. Mat.* **2018**, doi:10.1002/adma.201802066.

[4] N. Elgrishi, M. B. Chambers, M. Fontecave, *Chem. Sci.* **2015**, *6*, 2522-2531.

[5] P. Kang, Z. Chen, A. Nayak, S. Zhang, T. J. Meyer, *Energy Environ. Sci.* **2014**, *7*, 4007-4012.

[6] J.-W. Wang, H.-H. Huang, J.-K. Sun, D.-C. Zhong, T.-B. Lu, *ACS Catal.* **2018**, *8*, 7612-7620.

[7] K. Lv, C. Teng, M. Shi, Y. Yuan, Y. Zhu, J. Wang, Z. Kong, X. Lu, *Adv. Funct. Mater.* **2018**, doi:10.1002/adfm.201802339.

[8] F. Marques Mota, D. L. T. Nguyen, J.-E. Lee, H. Piao, J.-H. Choy, Y. J. Hwang, D. H. Kim, *ACS Catal.* **2018**, *8*, 4364-4374.

[9] H. Mistry, R. Reske, Z. Zeng, Z.-J. Zhao, J. Greeley, P. Strasser, B. R. Cuenya, *J. Am. Chem. Soc.* **2014**, *136*, 16473-16476.

[10] D. L. T. Nguyen, M. S. Jee, D. H. Won, H. Jung, H.-S. Oh, B. K. Min, Y. J. Hwang, *ACS Sustain. Chem. Eng.* **2017**, *5*, 11377-11386.

[11] B. Qin, Y. Li, H. Fu, H. Wang, S. Chen, Z. Liu, F. Peng, *ACS Appl. Mater. Interfaces* **2018**, *10*, 20530-20539.

[12] M. B. Ross, C. T. Dinh, Y. Li, D. Kim, P. De Luna, E. H. Sargent, P. Yang, *J. Am. Chem. Soc.* **2017**, *139*, 9359-9363.

[13] W. Sheng, S. Kattel, S. Yao, B. Yan, Z. Liang, C. J. Hawxhurst, Q. Wu, J. G. Chen, *Energy Environ. Sci.* **2017**, *10*, 1180-1185.

[14] F. Urbain, P. Tang, N. M. Carretero, T. Andreu, L. G. Gerling, C. Voz, J. Arbiol, J. R. Morante, *Energy Environ. Sci.* **2017**, *10*, 2256-2266.
[15] R. He, A. Zhang, Y. Ding, T. Kong, Q. Xiao, H. Li, Y. Liu, J. Zeng, *Adv. Mat.* **2018**, *30*, 1705872.
[16] J. He, N. J. J. Johnson, A. Huang, C. P. Berlinguette, *ChemSusChem* **2018**, *11*, 48-57.
[17] M. Watanabe, M. Shibata, A. Kato, M. Azuma, T. Sakata, *J. Electrochem. Soc.* **1991**, *138*, 3382-3389.
[18] H.-C. Shin, M. Liu, *Chem. Mat.* **2004**, *16*, 5460-5464.
[19] H. C. Shin, J. Dong, M. Liu, *Adv. Mat.* **2003**, *15*, 1610-1614.
[20] J. Rosen, G. S. Hutchings, Q. Lu, R. V. Forest, A. Moore, F. Jiao, *ACS Catal.* **2015**, *5*, 4586-4591.
[21] *CRC Handbook of Chemistry and Physics, 99th Edition*, CRC Press **2018**.
[22] M. R. Thorson, K. I. Siil, P. J. A. Kenis, *J. Electrochem. Soc.* **2013**, *160*, F69-F74.
[23] Y. Lum, B. Yue, P. Lobaccaro, A. T. Bell, J. W. Ager, *J. Phys. Chem. C* **2017**, *121*, 14191-14203.
[24] Y. Hori, in *Modern Aspects of Electrochemistry* (Eds.: C. G. Vayenas, R. E. White, M. E. Gamboa-Aldeco), Springer New York, New York, NY, **2008**, pp. 89-189.
[25] A. Bagger, W. Ju, A. S. Varela, P. Strasser, J. Rossmeisl, *ChemPhysChem* **2017**, *18*, 3266-3273.
[26] D. Ren, B. S.-H. Ang, B. S. Yeo, *ACS Catal.* **2016**, *6*, 8239-8247.
[27] S. Ma, M. Sadakiyo, M. Heima, R. Luo, R. T. Haasch, J. I. Gold, M. Yamauchi, P. J. A. Kenis, *J. Am. Chem. Soc.* **2017**, *139*, 47-50.
[28] A. D. McNaught, A. Wilkinson, (Eds.: M. Nic, J. Jirat, B. Kosata), IUPAC, **2006**, https://doi.org/10.1351/goldbook.R05419.

Entry for the Table of Contents

FULL PAPER

Two is better than one: a series of bimetallic Zn-Cu electrodes were prepared and used for syngas production by CO_2 electroreduction, allowing a broad range of H_2:CO ratios to be obtained independently of the potential applied.

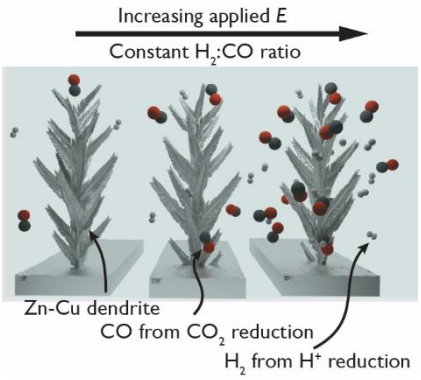

Sarah Lamaison, David Wakerley, David Montero, Gwenaëlle Rousse, Dario Taverna, Domitille Giaume, Huan Ngoc Tran, Marc Fontecave and Victor Mougel**

Page No. – Page No.

Zn-Cu alloy nanofoams as efficient catalysts for CO_2 reduction to syngas mixtures with potential-independent H_2:CO ratio